Journal of Catalysis 283 (2011) 133–142

Contents lists available at SciVerse ScienceDirect

Journal of Catalysis

journal homepage: www.elsevier.com/locate/jcat

The relationship between the structural properties of bimetallic Pd–Sn/SiO_2 catalysts and their performance for selective citral hydrogenation

Aurélie Vicente [a,1], Gwendoline Lafaye [a], Catherine Especel [a,*], Patrice Marécot [a], Christopher T. Williams [b]

[a] Laboratoire de Catalyse en Chimie Organique, UMR 6503, Université de Poitiers, 40 avenue du Recteur Pineau, 86022 Poitiers Cedex, France
[b] Department of Chemical Engineering and NanoCenter, University of South Carolina, Columbia, SC 29208, United States

ARTICLE INFO

Article history:
Received 18 February 2011
Revised 21 July 2011
Accepted 30 July 2011
Available online 6 September 2011

Keywords:
Pd
Sn
Silica
Bimetallic catalysts
Selective hydrogenation

ABSTRACT

The effect of Sn addition to Pd on the selective liquid-phase hydrogenation of citral to α,β-unsaturated alcohols (UA: nerol and geraniol) was examined. Pd–Sn/SiO_2 bimetallic catalysts were prepared by successive impregnation method and were characterized by transmission electronic microscopy (TEM) coupled with energy dispersive X-ray spectroscopy (EDX), temperature-programmed reduction (TPR), Fourier transform infrared (FTIR) spectroscopy of adsorbed CO, and X-ray photoelectron spectroscopy (XPS). Sn addition to Pd/SiO_2 catalysts significantly modifies their properties for citral hydrogenation performed at 130 °C, under 7 MPa and in isopropanol solvent, inducing a promoting effect on the UA selectivity. This promoting effect is related to the existence of a Pd–Sn interaction highlighted by EDX analysis, TPR under hydrogen and FTIR of adsorbed CO. The latter technique suggested the presence of a geometric effect on catalytic activity. Maximum UA selectivities (>75% at 30% citral conversion) were obtained when an alloy of the Pd_3Sn type is formed in the bimetallic particles, as confirmed by TPR and XPS. Moreover, FTIR measurements of the adsorbed CO singleton frequency as well as XPS binding energy shifts strongly imply an electron transfer from Sn to Pd, which is proposed to be responsible for enhanced adsorption of citral C=O bond on the surface of Pd–Sn/SiO_2 bimetallic catalysts. To our knowledge, it is the first time that modified Pd catalysts lead to such important UA selectivity values during α,β-unsaturated aldehyde hydrogenation.

1. Introduction

The selective hydrogenation of α,β-unsaturated aldehydes is a very important reaction for the synthesis of various fine chemicals products, in particular α,β-ethylenic alcohols, which are terpenic compounds used in the food, fragrance and pharmaceutical industries [1–3]. With a single-metal catalyst, the formation of α,β-ethylenic alcohols is a difficult task, with the C=O bond reduction depending on various types of factors. First, the structure of the molecule to be reduced can lead to possible steric hindrance around the C=O bond [4–6]. Second, geometric factors such as metal dispersion and surface morphology, coupled with the support structure and pore accessibility, play important roles [7,8]. Finally, electronic effects arise from the differential electron density of metal particles that can be controlled by varying the metal particle size and/or by addition of a modifier [9,10].

Metal catalysts containing noble metals (e.g., Pt, Pd) are known to be active in C=C hydrogenation but not for C=O hydrogenation. Such catalysts easily lead to saturated aldehydes or saturated alcohols with a poor unsaturated alcohol (UA) selectivity. However, the modification of noble metals by a second inactive one (e.g., Pb, Sn, Ge, etc.) [11–17] or the use of a reducible support (e.g., TiO_2) [18–26] can favor the formation of α,β-ethylenic alcohols. The molecules most often used as model compounds in catalytic studies are cinnamaldehyde (C_6H_5—CH=CH—CHO), crotonaldehyde (CH_3—CH=CH—CHO) and citral ((CH_3)$_2$—C=CH—CH_2—CH_2—C(CH_3)=CH—CHO), the last of which is explored in this study. Several reviews presented the state of art in the selective reduction of α,β-unsaturated aldehydes, describing the recent development in catalyst structures, catalyst characterization techniques as well as kinetic aspects in order to achieve tailor-made catalysts for this kind of reaction [2,27,28]. Singh and Vannice studied citral hydrogenation on various M/SiO_2 catalysts with M metals belonging to groups 8–10 of the periodic table [29]. The activity of the various metals expressed in turnover frequency (TOF) is as follows: Pd > Pt > Ir > Os > Ru > Rh > Ni > Co ≫ Fe. Good UA selectivity (S_{UA}) is attained with Os, Ru, and Co, while Rh, Ni, and Pd are highly unselective. The different UA selectivities observed on these metals were addressed using theoretical calculations by Delbecq and Sautet [30]. These authors suggested that C=C adsorption is hindered by a more broad metal d band. Indeed, the d band width

* Corresponding author. Fax: +33 (0)5 49 45 37 41.
E-mail address: catherine.especel@univ-poitiers.fr (C. Especel).
[1] Current address: Laboratoire de Catalyse et Spectrochimie de Caen, EnsiCaen, Université de Caen, 6 Boulevard Maréchal Juin, 14050 Caen Cedex, France.

0021-9517/$ - see front matter © 2011 Elsevier Inc. All rights reserved.
doi:10.1016/j.jcat.2011.07.010

decreases as follows: Os ≈ Ir > Pt > Pd, in agreement with the UA selectivities classification. In addition to metal specificities, these authors also found by studying the adsorption of various α,β-unsaturated aldehydes on platinum and palladium crystal faces that the adsorption mode of the substrate is strongly dependent on the type of surface structure exposed.

Thus, Pd is well known to be very active for the C=C function saturation during α,β-unsaturated aldehyde hydrogenation, but is considered unselective for hydrogenation of the C=O bond. With the aim of improving the selectivity toward the hydrogenation of the carbonyl bond, some authors have modified monometallic Pd catalysts by the addition of a second metal. Mahmoud and co-workers studied the influence of additives such as Ir, Cu, and Sn on sol–gel Pd/SiO_2 catalysts for cinnamaldehyde hydrogenation [31,32]. They did not observe a decrease in saturated aldehyde selectivity upon Ir or Cu addition onto Pd. In fact, in the case of the Cu, too high loading resulted in a total poisoning of the Pd active surface. On the other hand, a decrease in the saturated aldehyde selectivity was observed after Sn addition onto Pd, related to both geometric and electronic alloying effects. Such results were already obtained on supported Pt–Sn systems during the selective hydrogenation of the same α,β-unsaturated aldehyde [33]. Aramendía and co-workers studied selective liquid-phase hydrogenation of citral over Pd supported on a mixed 80:20 $SiO_2/AlPO_4$ system [34]. The presence of additives of the Lewis acid type such as $FeCl_2$ was found to considerably alter the hydrogenation mechanism. Under these experimental conditions, the selectivity was proved to be strongly dependent on the Fe^{2+}/Pd atomic ratio. They obtained the best results for a ratio equal to unity, with the S_{UA} reaching 35% for 25% citral conversion. More recently, Liu et al. reported the presence of significant synergistic effects on $Pd–Au/TiO_2$ bimetallic catalysts during the selective hydrogenation of citral [26]. These synergistic effects contribute mainly to the enhancement of the conversion rate and of the citronellal selectivity, but the hydrogenation of the carbonyl function was not modified.

In the present work, SiO_2-supported bimetallic catalysts containing Pd and Sn were studied for the citral hydrogenation in a batch reactor, under hydrogen pressure and in isopropanol as solvent. The objectives of this study are the following: (i) to succeed in synthesizing a series of Pd-based bimetallic catalysts higher selective for the formation of unsaturated alcohols (UA: nerol and geraniol) than the Pd-based systems described until now in the literature; (ii) to characterize the as-synthesized Pd–Sn catalysts with a view towards unraveling the role of the Sn modifier.

2. Experimental

2.1. Catalyst preparation

A silica (from Degussa) with a specific surface area of 180 m^2/g and a pore volume of 0.47 cm^3/g was used as support. Prior to its use, it was ground and sieved in order to retain particles with sizes between 0.04 and 0.10 mm, and calcined in flowing air at 500 °C for 4 h. 1.0 wt% Pd/SiO_2 monometallic catalysts were prepared by wet impregnation of the support at room temperature using a solution of $Pd(acac)_2$ in acetone. The monometallic catalysts were dried overnight at 120 °C, then calcined in flowing air at 300 °C for 2 h, and finally reduced under hydrogen flow at 300 °C or 500 °C for 1 h. Bimetallic $Pd–Sn/SiO_2$ catalysts were prepared by successive impregnations of the precursor salts without intermediate activation: after impregnation of $Pd(acac)_2$ in acetone onto SiO_2, the catalyst was dried at 120 °C overnight, then a $SnBu_4$ solution in *n*-heptane was impregnated and the resulting catalysts were dried overnight at 120 °C. Finally, the bimetallic catalysts were successively calcined in air at 300 °C for 2 h and reduced under hydrogen flow either at 300 °C or at 500 °C for 1 h (2 °C/min heating rate).

2.2. Transmission electron microscopy (TEM) measurements

Transmission electron microscopy (TEM) studies were performed on a Philips CM 120 instrument operating at 120 kV. All the samples were embedded in a polymeric resin (spur) and cut into a section as small as 40 nm with an ultramicrotome equipped with a diamond knife. Cuts were then deposited on an Al grid previously covered with a thin layer of carbon. Average particle sizes were determined by measuring at least 100 particles for each sample analyzed, from at least five different micrographs, and using the following formula: $\bar{d} = \sum n_i d_i^3 / \sum n_i d_i^2$ (d_i = diameter of the particle n_i). Microanalysis of Pd and Sn was carried out by energy dispersive X-ray spectroscopy (EDX) in the nanoprobe mode.

2.3. Hydrogen chemisoprtion

The metallic accessibility or dispersion (*D*%) was determined from H_2 chemisorption measurement, carried out in a pulse chromatographic system, using a stoichiometry of $H/Pd_{surface} = 1$. For all the catalysts, the H_2 chemisorption measurement was carried out at 70 °C, since at this temperature there is no formation of β-Pd hydride phase by diffusion of hydrogen into the metal [35]. The metal particle size was calculated from the dispersion *D* (%) using the classical hypothesis of cubic particles with one face in contact with the support (five faces exposed to the gases), and considering an equidistribution of the (1 0 0), (1 1 0) and (1 1 1) faces.

2.4. Temperature-programmed reduction (TPR) experiments

Two successive TPR experiments were performed with a 1.0 vol% H_2/Ar gas mixture. The temperature range was 25–500 °C with a ramp of 5 °C/min and then maintained at 500 °C for 1 h. The hydrogen uptake was monitored by a thermal conductivity detector. Prior to the first TPR, the monometallic and bimetallic catalysts after impregnation and drying were first pretreated *in situ* under oxygen for 30 min at 300 °C and cooled down to room temperature. Thus, the reduction performed in the TPR apparatus corresponds to the first reduction step undergone by the tested samples. After the first TPR experiment, a second one was performed following the same protocol.

2.5. Fourier transform infrared (FTIR) spectroscopy study of adsorbed CO

Transmission FTIR spectra were collected in the single beam mode, with a resolution of 2 cm^{-1}, using a Nicolet Nexus 470 FT-IR spectrometer equipped with an MCT-B detector. A 10-cm-long stainless steel IR cell, with NaCl windows cooled by flowing water was used to collect *in situ* spectra. A heating element wrapped around the cell allowed spectra collection at elevated temperatures. The cell temperature was monitored by a thermocouple placed in close proximity with the catalyst sample. Reference spectra of the clean surfaces in N_2 were collected at room temperature. Difference spectra between the samples and the corresponding reference are shown in this paper. Catalyst samples were prepared as self-supported wafers with a diameter of 12 mm containing approximately 20 mg/cm^2.

Prior to CO adsorption experiments, all catalysts were reduced *in situ* for 1 h under H_2 at 300 °C or 500 °C, according to the activation protocol used during their preparation. Following this reduction step, the samples were flushed with N_2 at the reduction temperature and cooled in N_2 to room temperature. At room temperature, a flowing 1% CO/He mixture was introduced to the

cell and spectra were collected until steady state was reached. N_2 was then purged through the cell to remove any weakly bonded CO.

Spectral deconvolution was performed using the Galactic PeakSolve peak-fitting program. All deconvoluted spectra shown in this paper are converged solutions, with correlation factors above 0.999 and standard errors below 0.004.

2.6. X-ray photoelectron spectroscopy (XPS)

X-ray photoelectron spectroscopy (XPS) measurements were collected using a hemispherical analyzer on a Kratos Axis Ultra DLD XPS with a monochromated Al Kα X-ray source. In a pretreatment cell directly attached to the XPS chamber, catalysts were pretreated *in situ* in H_2 atmosphere during 1 h at the same temperature that during their initial reduction. The samples were then cooled to room temperature and moved without exposure to air into the ultra-high-vacuum chamber (10^{-9} torr). Peak fitting was achieved using XPSPeak 4.1 software. All Pd and Sn binding energies were calibrated with respect to Si 2p (103.3 eV) and were then modeled using a mixed Shirley-Linear background. Elemental surface stoichiometries were obtained from peak area ratios corrected by appropriate sensitivity. Gaussian/Lorenzian sum functions were used to fit the line shapes of the Pd 3d and Sn 3d peaks.

2.7. Citral hydrogenation

The liquid-phase hydrogenation of citral was carried out in a 300-mL stirred autoclave (Autoclave Engineers, fitted with a system for liquid sampling) at 130 °C and at constant pressure of 7 MPa. Pre-reduced catalysts were immersed into 90 mL of solvent (isopropanol 99%) without exposure to air before introduction into the autoclave. After a first flush with nitrogen and a second with hydrogen, the temperature was raised to 130 °C under 3 MPa of hydrogen. Then a mixture of substrate (3 mL of citral) and of isopropanol (10 mL) was loaded into the autoclave through a cylinder under a 7-MPa hydrogen pressure. Zero time was taken at this moment and stirring was switched on. The reaction time was modulated in order to obtain a final conversion value enough to determine the unsaturated alcohols (UA) selectivity at a given citral conversion similar for all the samples. In this study, the UA selectivities will be given at 30% citral conversion, which implied to perform hydrogenation tests during 6 h for the less active catalysts. Liquid samples were analyzed by gas chromatography on a Thermofinnigan chromatograph equipped with an FID detector and a capillary column DB-WAX (J&W, 30 m, 0.53 mm i.d.) using nitrogen as carrier gas.

3. Results

3.1. Preliminary characterization of Pd/SiO_2 and $Pd–Sn/SiO_2$ catalysts

The characteristics of the 1 wt% Pd monometallic and 1 wt% Pd–*x* wt% Sn bimetallic catalysts supported on SiO_2 are summarized in Table 1. Examples of TEM images obtained for the 1 wt% Pd–1.5 wt% Sn/SiO_2 sample, as well as the corresponding size distributions, are represented in Fig. 1 for both reduction temperatures. In the case of the monometallic Pd/SiO_2 samples, the metallic particle size was determined by hydrogen chemisorption, since TEM analysis revealed the presence of particles with very inhomogeneous sizes, making difficult their precise inventory. For all systems, an increase in the reduction temperature from 300 °C to 500 °C resulted in some sintering of the metallic particles. However, this sintering phenomenon was less marked in the case of the bimetallic catalysts. For example, the average particle size increases from 5.9 nm (reduction at 300 °C) to 8.1 nm (reduction at 500 °C) for the 1 wt% Pd–1.5 wt% Sn/SiO_2 bimetallic catalyst, whereas it increased from 8.0 nm to 13.6 nm for the monometallic system. In addition, it should be noted that after reduction at a given temperature, the bimetallic catalysts have average particle sizes lower than that of monometallic catalyst. Thus, for bimetallic samples, the presence of Sn allows one to maintain Pd in a more divided state on silica support. Lastly, EDX analysis, performed with a probe of appropriate diameter in order to survey only one particle under the electron beam, proves the presence of both Pd and Sn atoms inside particles. Consequently, Sn is in contact with Pd in the bimetallic catalysts proving the existence of a bimetallic interaction.

Table 1
Characteristics of the 1.0 wt% Pd monometallic and 1.0 wt% Pd–*x* wt% Sn bimetallic catalysts supported on SiO_2.

Catalyst/SiO_2	$T_{reduction}$ (°C)	Average particle size (nm)	H_2 consumption during first TPR (μmol $g^{-1}_{catalyst}$)		H_2/Pd[c]
			T_{amb}–300 °C	T_{amb}–500 °C (1 h)	
1 wt% Pd	300	8.0[a]	96	96	1.02
	500	13.6[a]			
1 wt% Pd–1.0 wt% Sn	300	6.3[b]	115	142	1.22
	500	8.4[b]			
1 wt% Pd–1.3 wt% Sn	300	6.2[b]	n.d.	n.d.	n.d.
	500	8.2[b]			
1 wt% Pd–1.5 wt% Sn	300	5.9[b]	160	185	1.70
	500	8.1[b]			
1wt% Pd–1.7 wt% Sn	300	5.9[b]	n.d.	n.d.	n.d.
	500	8.0[b]			
1 wt% Pd–2.0 wt% Sn	300	5.7[b]	156	246	1.66
	500	8.0[b]			
2.0 wt% SnO_x	500	n.d.	12	72	–

n.d. = not determinated.
[a] Determined by hydrogen chemisorption.
[b] Determined by TEM.
[c] Deduced from H_2 consumption in the range T_{amb}–300 °C during first TPR.

In Fig. 2, TPR profiles of three $Pd–Sn/SiO_2$ bimetallic catalysts are compared with those of 1 wt% Pd/SiO_2 and 2 wt% SnO_x/SiO_2 monometallic catalysts. The hydrogen consumption amounts obtained from the curves of the first TPR are reported on Table 1. First, for the monometallic 1 wt% Pd/SiO_2 catalyst, the H_2/Pd ratio near the unity indicates that Pd is completely reduced from around 100 °C (the hydrogen consumption equal to 96 μmol $g^{-1}_{catalyst}$ corresponds to the theoretical consumption for the reduction of PdO phase, i.e. 94 μmol $g^{-1}_{catalyst}$). The two TPR profiles of 2 wt% SnO_x/SiO_2 monometallic catalyst show that it is difficult to reduce isolated Sn species deposited on silica, explaining the SnO_x oxide formula used to name this sample. Indeed, the reduction range begins only from 400 °C, and the total hydrogen consumption during the first TPR (72 μmol $g^{-1}_{catalyst}$) is much lower than the theoretical value for the reduction of the SnO_2 species to Sn^0 at 2 wt% Sn content (i.e. 337 μmol $g^{-1}_{catalyst}$). For the bimetallic catalysts, the profiles of the first TPR indicate the reduction of Sn species in contact with Pd, by the presence of hydrogen consumption after the main peak at low temperature and until 400 °C (i.e., the temperature required to initiate the reduction of isolated Sn). Thus, the TPR experiments clearly show the existence of a Pd–Sn bimetallic interaction, well evidenced by the second TPR. In fact, for the bimetallic samples, the second TPR leads to an increase of the H_2 consumption in the T_{amb}–400 °C range, indicating that the Sn species initially isolated on the support after impregnation remain in interaction with Pd after reduction. Moreover, like with the SnO_x/SiO_2 monometallic sample, all the Sn species are not completely reduced on the

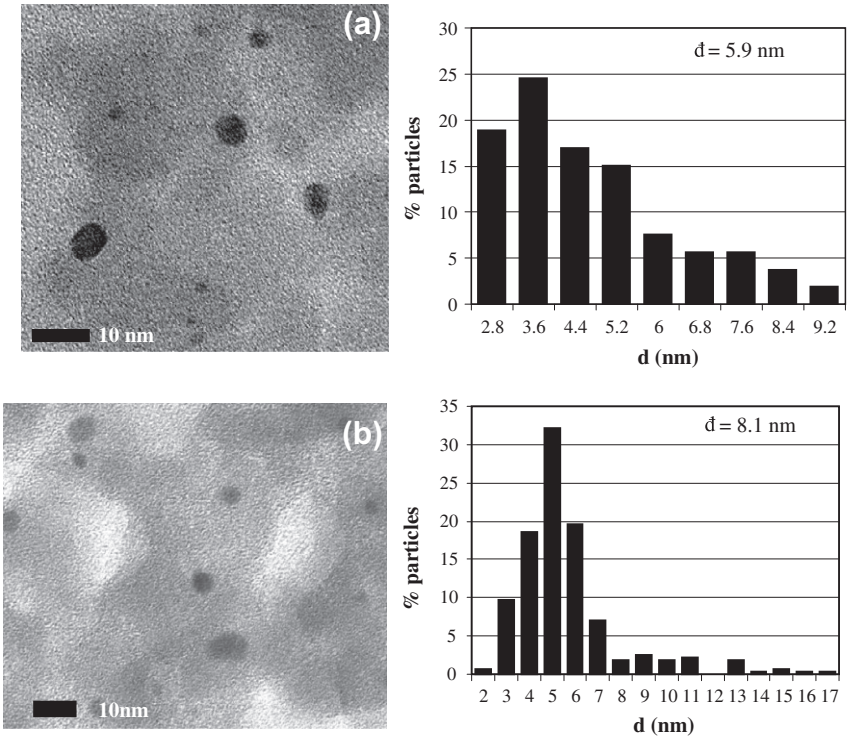

Fig. 1. TEM images and metal particle size distributions of 1 wt% Pd–1.5 wt% Sn/SiO_2 catalyst: (a) reduced at 300 °C, (b) reduced at 500 °C.

Pd–Sn/SiO_2 bimetallic catalysts even at 500 °C. This is suggested by the fact that the hydrogen consumption values (Table 1) never reach the theoretically required amounts for reduction of both PdO and SnO_2 oxides.

3.2. Catalytic performance during citral hydrogenation

Fig. 3 presents the main reaction pathways that can occur during citral hydrogenation. The reduction of citral can lead to a variety of products. A first step is the reduction of either the C=O or the conjugated C=C bond to produce geraniol and nerol, referred as unsaturated alcohols (UA), or citronellal, respectively. Consecutive hydrogenation leads to citronellol and finally to 3,7-dimethyloctanol. Apart from these reactions, secondary processes of cyclization or of reaction with the alcoholic solvent can lead to other by-products like isopulegol or acetals, respectively.

Fig. 4a represents the evolution of the citral conversion after 1 h reaction time according to the Sn content for the 1 wt% Pd–*x* wt% Sn/SiO_2 catalysts reduced at 300 °C and 500 °C. Under these experimental conditions, the Pd/SiO_2 catalysts are very active for citral hydrogenation, leading exclusively to the formation of C=C hydrogenated products, i.e., to an unsaturated alcohol (UA) selectivity equal to 0 (Fig. 4b). This behavior was predictable according to the literature results [26,29,34]. For the bimetallic catalysts series reduced at 300 °C (triangles), the addition of a low Sn content ($\leqslant$1 wt%) slightly modifies the conversion of the corresponding monometallic catalyst (Fig. 4a). For the highest Sn contents ($\geqslant$1 wt%), the citral conversion drops to reach approximately a 10% value. Concerning the Pd–Sn/SiO_2 catalysts reduced at 500 °C (squares), the citral conversion also decreases when Sn content increases, and thus from the lowest Sn content (1 wt%). Finally, the catalysts of this series with the highest Sn loadings present a conversion comparable with that of their counterparts reduced at 300 °C (near to 10%). For both series of catalysts, the UA selectivity strongly increases with the Sn content, reaching a maximum at 1.5 wt% Sn content before decreasing (Fig. 4b). For Sn contents higher than 1.3 wt%, the bimetallic catalysts reduced at 300 °C are slightly more selective than their counterparts reduced at 500 °C.

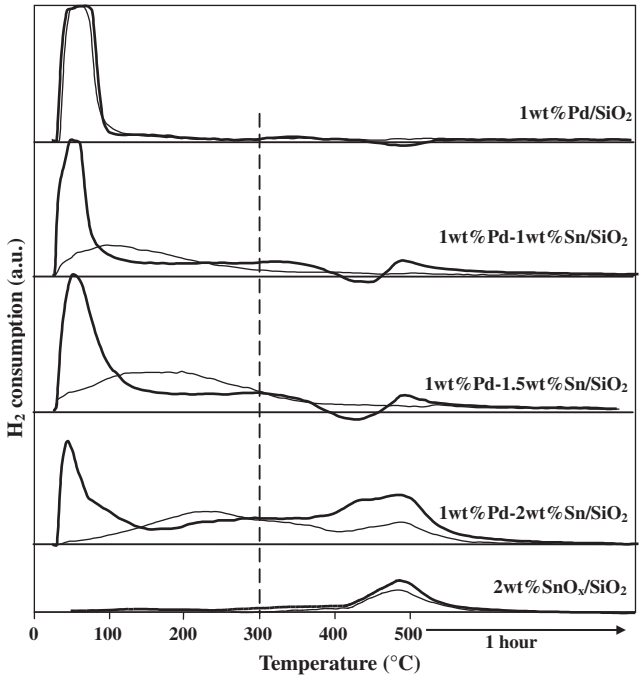

Fig. 2. TPR profiles of 1 wt% Pd/SiO_2 and 2 wt% SnO_x/SiO_2 monometallic catalysts and 1 wt% Pd–*x* wt% Sn/SiO_2 bimetallic catalysts after: (▬) calcination at 300 °C [first TPR], (—) calcination at 300 °C/reduction at 500 °C/calcination at 300 °C [second TPR].

3.3. FTIR study of adsorbed CO

Infrared spectra obtained after CO adsorption on the 1 wt% Pd monometallic and 1.0 wt% Pd–*x* wt% Sn bimetallic catalysts

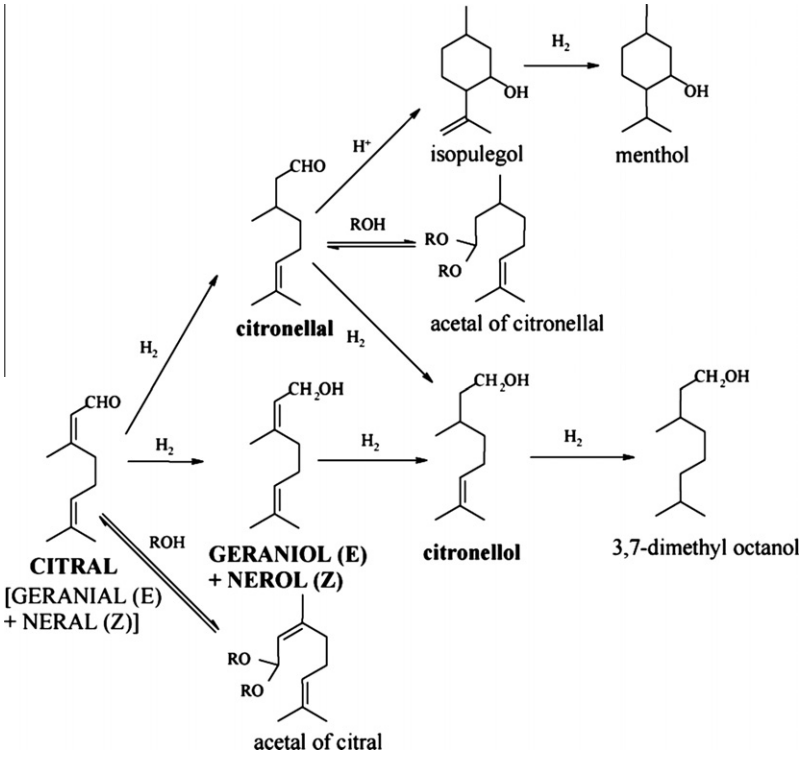

Fig. 3. Reaction scheme for citral hydrogenation.

supported on SiO_2 reduced at 300 °C and 500 °C are shown in Figs. 5 and 6. The spectral envelopes were deconvoluted into individual vibrational bands in order to identify the specific adsorbed species. Assignments of the various bands relating to adsorbed CO and their relative surface areas are summarized in Table 2.

The CO adsorption on Pd-based catalysts generally reveals two main regions: a first one between 2100 and 2030 cm^{-1} and a larger second one in the 2000–1800 cm^{-1} range. Whatever the reduction temperature of the monometallic Pd catalyst, deconvolution of the spectra revealed five distinct peaks (Figs. 5a and 6a): two peaks at ca 2095 and 2070 cm^{-1} and three peaks at 1991, 1952 and 1884 cm^{-1}. Similar results concerning the adsorption of CO on Pd are found in the literature, and allow the following attribution of the various bands observed [36–38]: (i) bands in the 2100–2070 and 2070–2050 cm^{-1} regions are attributed to linearly adsorbed Pd–CO species adsorbed on discontinuities between planes (i.e., corners, edges, steps, terraces), (ii) bands in the 1990–1950 cm^{-1} and 1940–1910 cm^{-1} regions indicate Pd_2–CO twofold bridging species adsorbed on (100) and (111) planes, respectively, (iii) the band in the 1880–1840 cm^{-1} region indicates Pd_3–CO threefold hollow site adsorption on (111) planes. The total adsorbed CO on the catalyst surface (S_{CO}) was estimated by taking the area under the entire band envelope in a given spectrum. The S_{CO} for both monometallic catalysts shows a decrease in the accessible sites with an increase in the reduction temperature, which is in perfect agreement with the values of the metal particles size obtained previously. Binet and co-workers used FTIR to study CO adsorption on Pd-supported catalysts presenting various dispersions [38]. They presented correlations between the dispersion values and the relative proportions of discontinuities, (111) faces and (100) faces. In the present work, the relative contributions from various species (indicated by the percentages in Table 2) for both monometallic catalysts and their average particle sizes deduced previously by H_2 chemisorption are in perfect agreement with the correlations established by these authors.

The results of the IR study for the bimetallic catalysts reduced at 300 °C (Fig. 5b–d) and 500 °C (Fig. 6b–d) show that the total S_{CO} decreases when the Sn content increases. Since Sn does not adsorb CO, this phenomenon indicates the presence of an increasing Sn quantity in contact with Pd. However, spectral deconvolution shows that the various adsorbed CO species are not affected in the same way (Table 2). The bridged species significantly decrease with increased Sn content compared with the linear species, which are in fact the majority species on the Pd–Sn/SiO_2 catalysts reduced at 500 °C. This behavior suggests a dilution effect of the Pd surface by Sn addition, which decreases the number of sites containing adjacent Pd atoms, and consequently the number of bridged adsorbed CO species [39].

3.4. XPS experiments

The curve-fitted XPS spectra of the Pd 3d and Sn 3d regions for the monometallic and bimetallic catalysts reduced at 300 °C are presented in Figs. 7 and 8, respectively. XPS analysis is known to give atomic compositions representative of the material surface until 10 nm in depth. Consequently, in the case of the studied monometallic and bimetallic catalysts presenting average particle sizes between 5.7 and 8.0 nm (after reduction at 300 °C, see Table 1), we can consider that the XPS results are here representative of the bulk composition.

In Fig. 7, the peaks observed at 332.0 eV and 337.5 eV correspond, respectively, to the Pd $3d_{5/2}$ and $3d_{3/2}$ core levels. For the purposes here, only the Pd $3d_{5/2}$ region will be considered. The fact that only one band is obtained in the $3d_{5/2}$ area indicates that all Pd is in the Pd^0 reduced form after reduction at 300 °C, in agreement with the TPR results (Section 3.1). The full-width-half-maximum (FWHM) of the Pd $3d_{5/2}$ peak given in Table 3 decreases with increasing Sn content, which implies an increase in the Sn quantity in contact with Pd [40]. Nevertheless, the FWHM obtained for bimetallic catalysts with Sn content $\geqslant$1.5 wt% are very close,

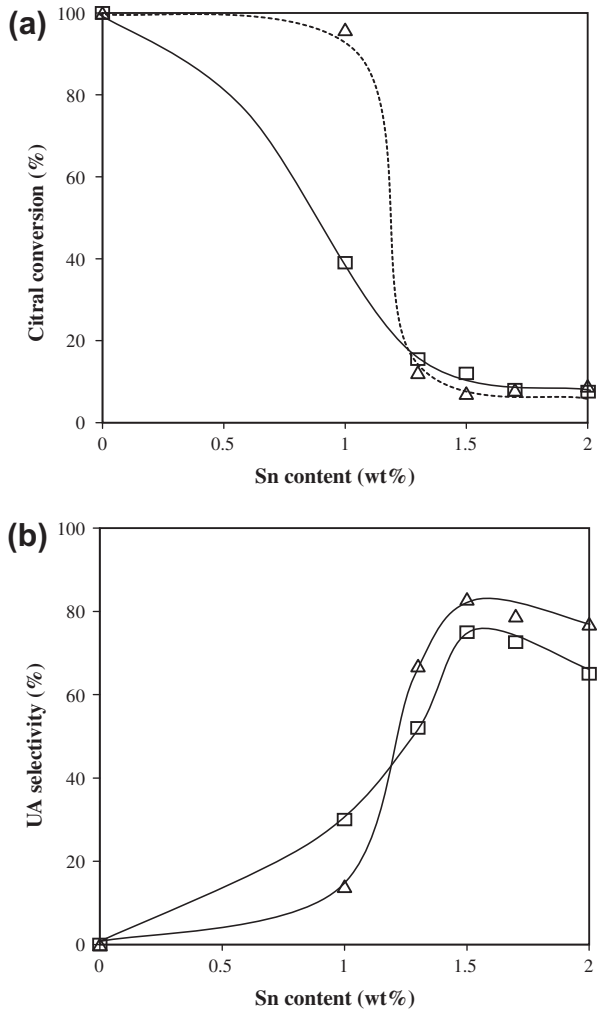

Fig. 4. (a) Citral conversion after 1 h reaction time and (b) unsaturated alcohols (UA) selectivity at 30% citral conversion as a function of Sn content for 1 wt% Pd–*x* wt% Sn/SiO_2 bimetallic catalysts: (△) reduced at 300 °C, (□) reduced at 500 °C.

suggesting that the Sn quantity in contact with Pd reaches a plateau, as previously observed from the hydrogen consumption during TPR experiments.

The spectra of the bimetallic catalysts in Fig. 8 show two mean peaks at 485.0 eV and 493.3 eV, attributed respectively to the Sn $3d_{5/2}$ and $3d_{3/2}$ core levels. Once again, only the Sn $3d_{5/2}$ peak will be further discussed here. This lower binding energy peak is decomposed into two contributions. In agreement with literature [15,16,40,41], the contribution located at 485.0 eV corresponds to oxidized Sn (Sn^{2+} and/or Sn^{4+}), whereas the one at lower binding energy (482.0 eV) is assigned to reduced Sn. Unfortunately, XPS cannot discriminate between Sn^{2+} and Sn^{4+} oxidized states [42]. After reduction at 300 °C, Fig. 8 indicates that oxidized Sn are always the prevailing Sn species whatever the Sn content of the bimetallic systems, in agreement with the results deduced from hydrogen consumption during TPR (Section 3.1).

Table 3 shows that the increase in the Sn content in the bimetallic systems leads to an increase in the Sn^0/Sn_{total} atomic ratio. Since the TPR results (cf. Fig. 2) show that 300 °C is not enough to reduce isolated supported Sn species, this trend indicates that the quantity of reduced Sn^0 species in contact with Pd increases with the Sn content for the catalysts treated at that temperature. Indeed, only 13% of Sn is reduced for bimetallic catalyst with 1 wt% Sn against 25% for the one with 1.5 wt% Sn. On the other

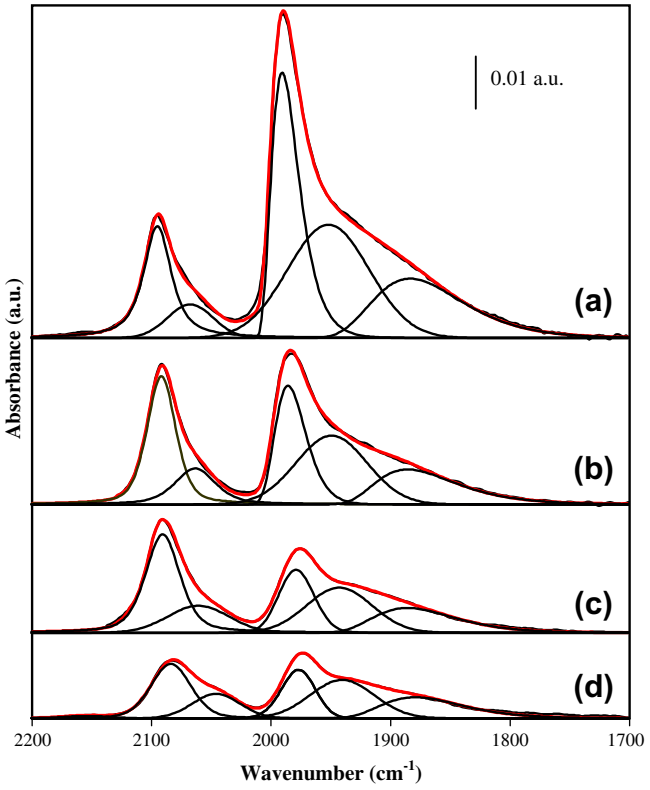

Fig. 5. FTIR spectra of adsorbed CO at room temperature on catalysts reduced at 300 °C: (a) 1 wt% Pd/SiO_2, (b) 1 wt% Pd–1 wt% Sn/SiO_2, (c) 1 wt% Pd–1.5 wt% Sn/SiO_2, (d) 1 wt% Pd–2 wt% Sn/SiO_2.

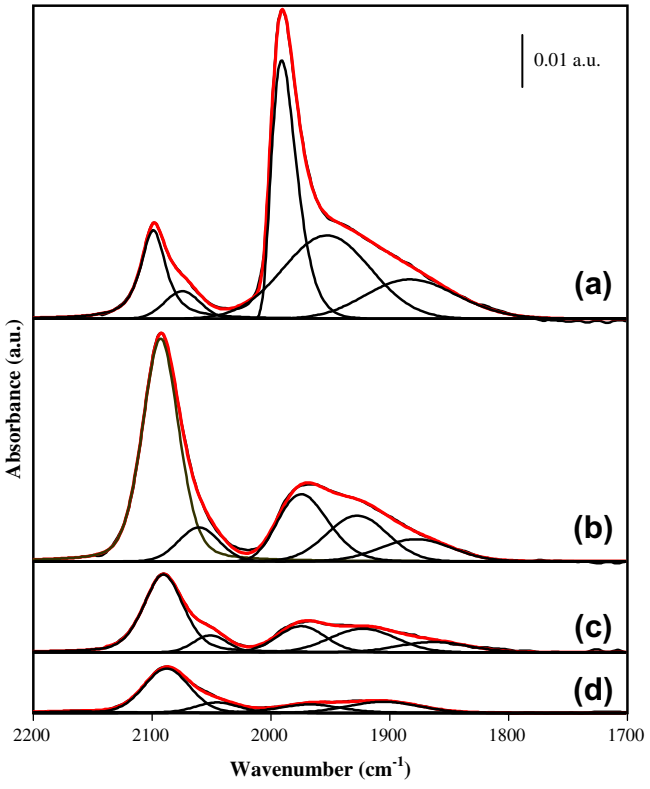

Fig. 6. FTIR spectra of adsorbed CO at room temperature on catalysts reduced at 500 °C: (a) 1 wt% Pd/SiO_2, (b) 1 wt% Pd–1 wt% Sn/SiO_2, (c) 1 wt% Pd–1.5 wt% Sn/SiO_2, (d) 1 wt% Pd–2 wt% Sn/SiO_2.

Table 2
Peak assignments (cm^{-1}) and relative contributions (%) for each peak observed during the adsorption of CO on 1.0 wt% Pd monometallic and 1.0 wt% Pd–*x* wt% Sn bimetallic catalysts supported on SiO_2 ($\theta_{CO} = 1$). S_{CO} indicates the total integrated area under the curve.

Catalyst/SiO_2	S_{CO}	Linear Pd–CO		Bridged Pd_2–CO on (100) faces	Bridged Pd_2–CO on (111) faces	Bridged Pd_3–CO on (111) faces
Reduced at 300 °C						
1 wt% Pd	6.2	2095	2068	1991	1952	1884
		14%	*6%*	*28%*	*32%*	*20%*
1 wt% Pd–1.0 wt% Sn	4.3	2092	2064	1986	1949	1886
		24%	*10%*	*21%*	*28%*	*17%*
1 wt% Pd–1.5 wt% Sn	3.1	2091	2061	1979	1943	1886
		31%	*13%*	*17%*	*23%*	*16%*
1 wt% Pd–2.0 wt% Sn	2.1	2084	2046	1977	1941	1879
		25%	*12%*	*18%*	*26%*	*19%*
Reduced at 500 °C						
1 wt% Pd	4.5	2099	2075	1991	1953	1883
		14%	*5%*	*31%*	*34%*	*16%*
1 wt% Pd–1.0 wt% Sn	3.9	2093	2061	1974	1927	1878
		50%	*8%*	*18%*	*15%*	*9%*
1 wt% Pd–1.5 wt% Sn	1.4	2091	2051	1974	1923	1863
		46%	*8%*	*16%*	*20%*	*10%*
1 wt% Pd–2.0 wt% Sn	0.9	2088	2045	1967	1906	–
		53%	*13%*	*15%*	*19%*	

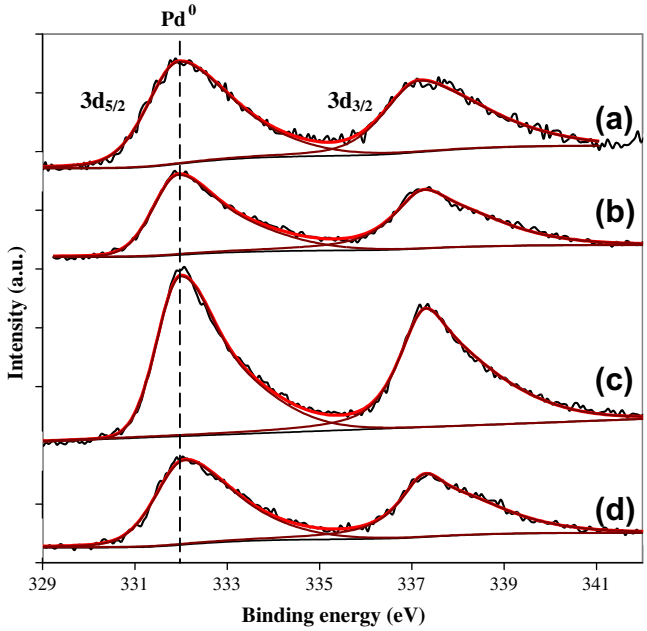

Fig. 7. Pd 3d spectra of the catalysts reduced at 300 °C: (a) 1 wt% Pd/SiO_2, (b) 1 wt% Pd–1 wt% Sn/SiO_2, (c) 1 wt% Pd–1.5 wt% Sn/SiO_2, (d) 1 wt% Pd–2 wt% Sn/SiO_2.

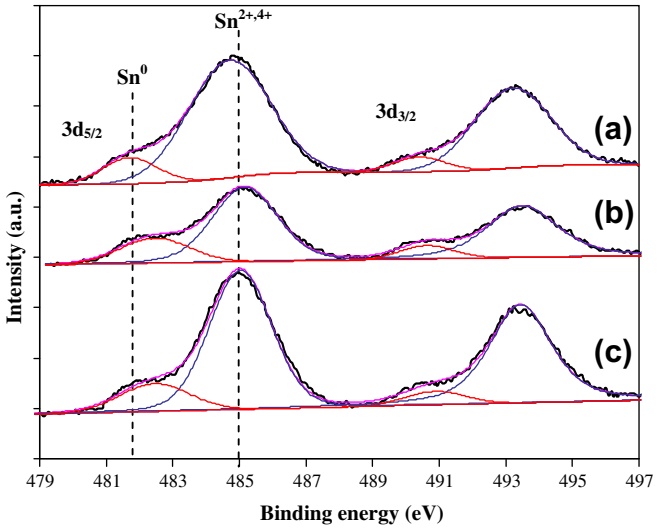

Fig. 8. Sn 3d spectra of the catalysts reduced at 300 °C: (a) 1 wt% Pd–1 wt% Sn/SiO_2, (b) 1 wt% Pd–1.5 wt% Sn/SiO_2, (c) 1 wt% Pd–2 wt% Sn/SiO_2.

hand, the bimetallic sample with 2 wt% Sn presents only 17% of reduced Sn. Thus, as Sn is added to Pd above 1.5 wt%, the quantity of Sn^0 species in contact with Pd particles would be constant. This allows an estimation of 0.37 wt% Sn^0 and 0.34 wt% Sn^0 for the 1 wt% Pd–1.5 wt% Sn/SiO_2 and 1 wt% Pd–2 wt% Sn/SiO_2 catalysts, respectively.

4. Discussion

The objective of this study was to modify the catalytic properties of Pd with the aim of improving the selectivity toward the hydrogenation of the citral carbonyl bond. Indeed, as described previously, Pd is known to be very active in hydrogenation of the C=C function but not at all selective for C=O hydrogenation. A 1 wt% Pd/SiO_2 catalyst reduced at 300 °C or 500 °C was modified by Sn addition, and evaluated in citral hydrogenation at 130 °C, under hydrogen pressure (7 MPa) in isopropanol as solvent. The TEM and H_2 chemisorption analysis show the presence of large Pd particles on the monometallic catalysts. These results suggest a strong mobility of Pd on the silica surface during the activation treatments, and are in accord with reports of weak metal-support interactions [43]. Nevertheless, the Sn addition induces a better Pd dispersion on the silica support, since the mean metal particle sizes in the bimetallic samples are lower than those in the corresponding monometallic catalyst (Table 1). The same phenomenon was already observed on Rh–Ge/SiO_2 and Pd–Sn/Al_2O_3 catalysts by TEM and $O_2/H_2/O_2$ titration experiments [43,44]. The presence of Sn species dispersed on the silica support may hinder the mobility of Pd particles explaining then the higher dispersion for tin containing catalysts compared with monometallic sample after reduction at 300 °C, and in the same way the lower sintering effect after high temperature reduction on bimetallic catalysts.

Whatever the reduction temperature (300 °C or 500 °C) or the Sn content (1–2 wt%) of the bimetallic catalysts, a Pd–Sn interaction is highlighted by EDX analysis as well as by TPR experiments. Isolated Sn species are also present on the silica support as

Table 3
Binding energy (eV) of Pd $3d_{5/2}$ and Sn $3d_{5/2}$ core levels and atomic surface ratios obtained by XPS for 1.0 wt% Pd monometallic and 1.0 wt% Pd–*x* wt% Sn bimetallic catalysts supported on SiO_2, reduced at 300 °C.

Catalyst/SiO_2	1 wt% Pd	1 wt% Pd–1 wt% Sn	1 wt% Pd–1.5 wt% Sn	1 wt% Pd–2 wt% Sn
Pd^0 $3d_{5/2}$ (eV)	331.9	331.8	332.0	332.1
(FWHM)	(1.80)	(1.58)	(1.36)	(1.34)
Sn^0 $3d_{5/2}$ (eV)	–	482.0	482.5	482.5
$Sn^{2+,4+}$ $3d_{5/2}$ (eV)	–	485.0	485.2	485.0
Sn^0/Sn_{total}	–	0.13	0.25	0.17
Sn_{total}/Pd	–	1.57	1.26	2.40
$Sn^0/[Sn^0 + Pd]$	–	0.17	$0.25 \approx Pd_3Sn$	$0.29 \approx Pd_3Sn$

indicated by the H_2 consumption after 400 °C on the TPR profiles of the bimetallic catalysts, like in the case of the SnO_x/SiO_2 sample (Fig. 2). The quantitative exploitation deduced from curves of the first TPR of bimetallic catalysts (Table 1) indicates that the hydrogen consumption increases with the Sn content compared with the 1 wt% Pd/SiO_2 monometallic sample. However, a great proportion of Sn is not reduced to the zero oxidation state, according to the difference between the theoretical and experimental hydrogen consumptions. A plateau of consumption in the T_{amb}–300 °C range is obtained for the catalysts with Sn content $\geqslant$1.5 wt% (H_2/Pd ratio = 1.70 and 1.66). For these two samples, we can consider that the additional quantity of hydrogen consumed up to 300 °C is used to reduce the Sn^{4+} species to Sn^0. According to this hypothesis, only 0.38 and 0.36 wt% Sn is totally reduced in close contact with Pd for the 1 wt% Pd–1.5 wt% Sn/SiO_2 and 1 wt% Pd–2 wt% Sn/SiO_2 catalysts, respectively. These quantities of Sn^0 in contact with Pd^0 particles correspond to an alloy with a Pd_3Sn composition. For Pd–Sn/SiO_2 bimetallic catalysts with %Sn $\geqslant$ 1.5 wt%, all the Pd atoms are involved in this alloy formation.

During citral hydrogenation, as expected, the 1 wt% Pd/SiO_2 monometallic catalysts were very active for the C=C hydrogenation. Upon Sn addition, the activity decreased dramatically but the formation of unsaturated alcohol (UA) was observed, the selectivity towards these products increasing until a maximum with the additive content. Thus, at 30% citral conversion, the UA selectivity reached a maximum of 77% for the 1 wt% Pd–1.5 wt% Sn/SiO_2 catalyst reduced at 500 °C, and 82% for the same system reduced at 300 °C.

For the Pd–Sn/SiO_2 catalysts, the FTIR study of adsorbed CO shows that the Sn addition onto Pd results in a very marked geometrical effect, with a decrease in the total surface of adsorbed CO due mainly to the decrease in bridged Pd_B–CO species. This geometrical effect is explained by the dilution of surface Pd ensembles by Sn [39,45,46]. Moreover, it can be noticed in Table 2 that the Sn addition induces a notable shift of the peaks towards lower frequencies. Two effects can explain shifts towards lower wavenumbers: (i) a geometrical effect whereby Pd dilution by Sn induces a decrease in dipole–dipole coupling between CO molecules and (ii) an electronic or ligand effect, due to a significant increase in the Pd–CO bond strength related to a higher extent of π backdonation from Pd to CO as defined in the Blyholder model [47]. As seen previously, a geometrical effect exists on the Pd–Sn/SiO_2 bimetallic systems, which is common for the case of a noble metal modified by an additive inactive for CO adsorption [41,48]. From the FTIR spectra performed at θ_{CO} = 1, it is not possible to conclude whether there is or not presence of an electronic effect. To elucidate this point, one technique in the literature consists of comparing the vibrational frequencies of linearly adsorbed CO at null CO coverage between a bimetallic catalyst and its monometallic counterpart [39,49]. In this case, a difference higher than 10 cm^{-1} reveals an electronic effect, i.e., a charge transfer between both metals of the bimetallic system.

To work at null CO coverage, carbon monoxide was desorbed under helium flow, first at room temperature during 30 min then at 50 °C. For both Pd–Sn/SiO_2 catalysts series, the evolution of the linear Pd–CO band wavenumbers was plotted according to θ_{CO}, values of which were calculated by dividing peak areas by the peak area obtained prior to any desorption. Results for the catalysts reduced at 500 °C are presented in Fig. 9. As can be seen, linear extrapolation to θ_{CO} = 0 yields the vibration frequency of the CO singleton (Table 4). It should be noted that the decomposition of the FTIR spectra reveals two individual peaks for the linear species which are both taken into account for the determination of the CO singleton frequency. Indeed, the wavenumbers given in Fig. 9 are obtained by a mathematical weighting of the wavenumbers of each of the two individual peaks.

Fig. 9 shows that the wavenumber decreases during the CO desorption indicating a reduction of the dipole–dipole effect between the CO molecules. In addition, Table 4 shows that the Sn addition to Pd induces a shift towards lower wavenumbers for the CO singleton ($\nu_{COlinear}$). This shift with regard to the Pd monometallic catalyst ($\nu_{mono} - \nu_{bi}$) is equal to 15 cm^{-1} for the sample containing 1 wt% Sn and increases with the Sn quantity. These results suggest the existence of an electronic effect between both metals, i.e., an electron transfer from Sn to Pd inducing an increase in Pd electronic density. This electron transfer appears to be more marked for the bimetallic catalyst with the higher Sn content (2 wt%).

The XPS results confirmed the presence of Sn species in a reduced state in contact with Pd on the bimetallic Pd–Sn/SiO_2 catalysts, with the Sn^0 quantity reaching a value of around 0.37 wt% for the systems with Sn content $\geqslant$1.5 wt%. In Table 3, it can be noticed that the binding energy of the Sn^0 $3d_{5/2}$ peak increases with the Sn content, from 482.0 eV to reach 482.5 eV for the bimetallic catalysts with %Sn $\geqslant$ 1.5 wt%. This upward shift of Sn^0 binding energy indicates an electron deficiency of Sn due to an electron

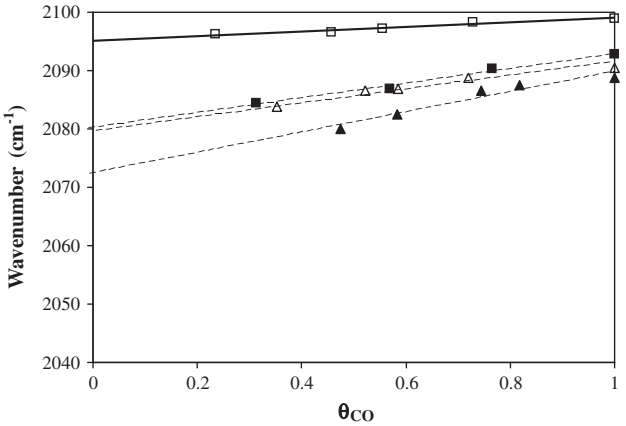

Fig. 9. Wavenumber of the linear Pd–CO species as a function of the CO coverage (θ_{CO}) for the monometallic and bimetallic catalysts reduced at 500 °C: (□) 1 wt% Pd/SiO_2, (■) 1 wt% Pd–1 wt% Sn/SiO_2, (△) 1 wt% Pd–1.5 wt% Sn/SiO_2, (▲) 1 wt% Pd–2 wt% Sn/SiO_2.

Table 4
Comparison between the vibration frequency of CO singleton of the 1 wt% Pd–*x* wt% Sn/SiO_2 catalysts and the one of the 1 wt% Pd/SiO_2 monometallic sample, reduced at 500 °C.

Catalyst/SiO_2	1 wt% Pd	1 wt% Pd–1 wt% Sn	1 wt% Pd–1.5 wt% Sn	1 wt% Pd–2 wt% Sn
$\nu_{COlinear}$ (cm^{-1})	2095	2080	2079	2072
Difference $\nu_{mono} - \nu_{bi}$ (cm^{-1})	–	15	16	23

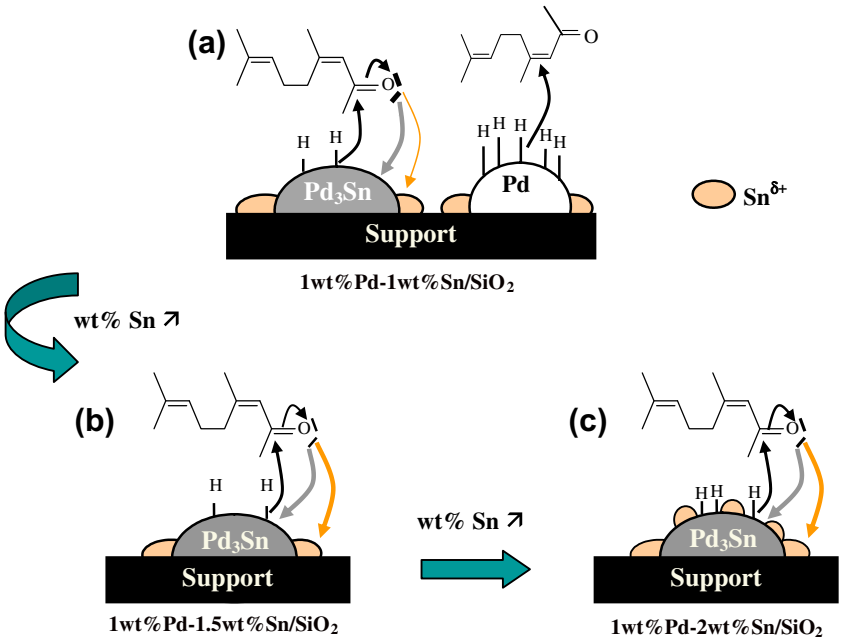

Fig. 10. Shematic representation of the adsorption modes of citral molecule on Pd–Sn/SiO_2 bimetallic catalysts depending on the Sn content.

transfer from Sn to Pd [15,41], which is in agreement with the above FTIR singleton frequency results. According to Jung and al. [50] and Sales and al. [45], this shift can be correlated with the formation of a Pd–Sn alloy. Indeed from the $Sn^0/(Sn^0 + Pd)$ atomic ratios, the formation of a Pd_3Sn composition phase can be suggested for the bimetallic catalysts with Sn content $\geqslant$1.5 wt% (given that all the Sn^0 species are in contact with Pd on bimetallic catalysts reduced at 300 °C). In addition, these bimetallic catalysts present the same binding energy for the Sn^0 peak (482.5 eV), suggesting that the same electron transfer between Pd and Sn exists on both samples, and so emphasizing the possible formation of the same Pd_3Sn alloy. The alloy formation between Pd and Sn is also confirmed by the decrease in the Sn_{total}/Pd atomic ratio when Sn content grows from 1 wt% to 1.5 wt% (Table 3) corresponding to a diffusion of Sn into Pd. On the other hand, this ratio increases for the 1 wt% Pd–2 wt% Sn/SiO_2 catalyst, while the Sn^0/Sn_{total} ratio decreases. This phenomenon suggests that the same Sn quantity diffuses into Pd on the 1 wt% Pd–1.5 wt% Sn/SiO_2 and 1 wt% Pd–2 wt% Sn/SiO_2 systems, with the excess of Sn deposited onto catalyst with 2 wt% Sn remaining mainly in oxidized form. Finally, the XPS results confirm the formation of a Pd_3Sn alloy on the 1 wt% Pd–*x* wt% Sn/SiO_2 bimetallic catalysts with $x \geqslant 1.5$ reduced at 300 °C, as already suggested from the TPR study.

The geometric and electronic modifications of Pd by Sn play a determinant role on the catalytic properties during citral hydrogenation, and allow one to explain the high selectivities to unsaturated alcohols (UA) observed on the Pd–Sn bimetallic systems. Fig. 10 presents schematic views of the bimetallic particles of the Pd–Sn/SiO_2 systems reduced at 300 °C according to the Sn content. The proposed citral adsorption modes are deduced from all the different characterization techniques in connection with the citral hydrogenation properties obtained on each Pd–Sn/SiO_2 bimetallic catalyst. For the bimetallic catalyst with the lowest Sn content (1 wt%), EDX, TPR, FTIR of adsorbed CO and XPS have revealed the presence of a Pd–Sn interaction. Nevertheless, this interaction does not result in the complete formation of the Pd_3Sn alloy in the bimetallic particles. The presence of some Pd_3Sn entities is not excluded but rather very limited, which explain why this system remains very active for citral hydrogenation but not very selective for C=O hydrogenation (S_{UA} = 13% at 30% citral conversion) (Fig. 10a).

In contrast, on Pd–Sn/SiO_2 bimetallic samples with %Sn $\geqslant$1.5 wt%, all the Pd atoms are in a Pd_3Sn alloy phase (Fig. 10b), favouring the hydrogenation of the carbonyl function but inducing a negative effect on the activity. The formation of this alloy allows the catalytic surface to fix selectively the oxygen atom of the C=O bond and leads to very selective catalysts for UA formation ($S_{UA\text{-}max}$ = 82% at 30% citral conversion for %Sn = 1.5 wt%). On the Pd_3Sn alloy surface of these supported bimetallic particles, Sn species are present in an oxidized form in a quantity that increases as the Sn content grows until 2 wt% (Fig. 10c). As for the Pd_3Sn alloy, $Sn^{\delta+}$ species appear to also contribute to activation of the citral C=O bond, but to a lesser extent. Indeed, the presence of a great quantity of these oxidized Sn entities must block part of the Pd_3Sn alloy active surface and then involves a slight decrease in the unsaturated alcohol selectivity for the 1 wt% Pd–2 wt% Sn/SiO_2 bimetallic catalyst (S_{UA} = 77% at 30% citral conversion), due to the formation of secondary products.

On Pd–Sn/SiO_2 bimetallic catalysts reduced at 500 °C, the same schematic representations can be proposed according to the Sn content, with different proportions of $Sn^{\delta+}$ species in contact with

Pd_3Sn alloy, and with probably a different oxidation state for these species.

5. Conclusion

This work was devoted to the study of Pd–Sn bimetallic catalysts with the aim of obtaining selective unsaturated alcohol catalysts for citral hydrogenation (α,β-unsaturated aldehyde) and elucidating the structure–property relationships in this system. On Pd-based systems (monometallic and bimetallic), very few studies are reported in literature concerning the selective hydrogenation of citral towards unsaturated alcohols (UA). Indeed, palladium is typically one of the worst metals for this reaction, since it is highly active to the reduction of the conjugated C=C bond.

The classical technique of successive impregnations was used for the preparation of the Pd–Sn/SiO_2 catalysts. During citral hydrogenation performed at 130 °C under 7 MPa and with isopropanol as solvent, the modification of Pd monometallic catalysts by Sn favoured the selective hydrogenation of conjugated C=O bond, leading to the formation of nerol and geraniol (UA).

The existence of Pd–Sn bimetallic interactions was confirmed by a suite of characterization techniques that included EDX analysis, TPR experiments, FTIR of adsorbed CO and XPS analysis. The quantity of Sn species reduced to Sn^0 state in contact with Pd deduced from the TPR characterization suggested the formation of a Pd_3Sn alloy for samples reduced at least at 300 °C. The formation of an alloy of such composition was also confirmed by XPS analysis. Moreover, this alloy induced an electron transfer from Sn towards Pd as evidenced by both FTIR measurement of CO singleton frequencies as well as by the XPS analysis. The presence of this Pd_3Sn alloy, which modifies the Pd sites both geometrically and electronically, is proposed to result in a significant deactivation of the sites responsible for C=C adsorption, while simultaneously providing new sites able to activate C=O bond of citral.

In conclusion, the Pd–Sn/SiO_2 catalysts synthesized in this work lead to important selectivities towards unsaturated alcohols (>80%) during citral hydrogenation. To our knowledge, it is the first time that such important selectivity values are observed on modified Pd catalysts for this kind of reaction.

References

[1] P. Claus, Top. Catal. 5 (1998) 51.
[2] P. Gallezot, D. Richard, Catal. Rev.-Sci. Eng. 40 (1998) 81.
[3] V. Ponec, Appl. Catal. A 149 (1997) 27.
[4] P. Beccat, J.C. Bertolini, Y. Gauthier, J. Massardier, P. Ruiz, J. Catal. 126 (1990) 451.
[5] Y. Nitta, K. Ueno, T. Imanaka, Appl. Catal. 56 (1989) 9.
[6] P. Gallezot, A. Giroir-Fendler, D. Richard, Catal. Lett. 5 (1990) 169.
[7] A. Giroir-Fendler, D. Richard, P. Gallezot, Catal. Lett. 5 (1990) 175.
[8] D.G. Blackmond, R. Oukaci, B. Blanc, P. Gallezot, J. Catal. 131 (1991) 401.
[9] C.E. Gigola, H.R. Aduriz, P. Bodnariuk, Appl. Catal. 27 (1986) 133.
[10] J.B. Boitiaux, J. Cosyns, S. Vasudevan, Appl. Catal. 15 (1985) 317.
[11] B. Coq, F. Figueras, C. Moreau, P. Moreau, M. Warawdekar, Catal. Lett. 22 (1993) 189.
[12] T.B.L.W. Marinelli, S. Nabuurs, V. Ponec, J. Catal. 151 (1995) 431.
[13] F. Coloma, A. Sepúlveda-Escribano, J.L.G. Fierro, F. Rodríguez-Reinoso, Appl. Catal. A 148 (1997) 63.
[14] I.M.J. Vilella, S.R. de Miguel, O.A. Scelza, J. Mol. Catal. A 284 (2008) 161.
[15] G. Neri, C. Milone, S. Galvagno, A.P.J. Pijpers, J. Schwank, Appl. Catal. A 227 (2002) 105.
[16] M.delC. Aguirre, P. Reyes, M. Oportus, I. Melían-Cabrera, J.L.G. Fierro, Appl. Catal. A 233 (2002) 183.
[17] G. Lafaye, T. Ekou, C. Micheaud-Especel, C. Montassier, P. Marecot, Appl. Catal. A 257 (2004) 107.
[18] M. Boutonnet Kizling, C. Bigey, R. Touroude, Appl. Catal. A 135 (1996) L13.
[19] D. Poondi, M.A. Vannice, J. Mol. Catal. A 124 (1997) 79.
[20] M.A. Vannice, D. Poondi, J. Catal. 169 (1997) 166.
[21] U.K. Singh, M.A. Vannice, J. Mol. Catal. A 163 (2000) 233.
[22] R. Malathi, R.P. Viswanath, Appl. Catal. A 208 (2001) 323.
[23] P. Reyes, H. Rojas, J.L.G. Fierro, Appl. Catal. A 248 (2003) 59.
[24] T. Ekou, A. Vicente, G. Lafaye, C. Especel, P. Marecot, Appl. Catal. A 314 (2006) 73.
[25] J.C. Serrano-Ruiz, A. Sepúlveda-Escribano, F. Rodríguez-Reinoso, D. Duprez, J. Mol. Catal. A 268 (2007) 227.
[26] R. Liu, Y. Yu, K. Yoshida, G. Li, H. Jiang, M. Zhang, F. Zhao, S. Fujita, M. Arai, J. Catal. 269 (2010) 191.
[27] K. Singh, M.A. Vannice, Appl. Catal. A 213 (2001) 1.
[28] P. Mäki-Arvela, J. Hájek, T. Salmi, D.Y. Murzin, Appl. Catal. A 292 (2005) 1.
[29] U.K. Singh, M.A. Vannice, J. Catal. 199 (2001) 73.
[30] F. Delbecq, P. Sautet, J. Catal. 152 (1995) 217.
[31] S. Mahmoud, A. Hammoudeh, S. Gharaibeh, J. Melsheimer, J. Mol. Catal. A 178 (2002) 161.
[32] A. Hammoudeh, S. Mahmoud, J. Mol. Catal. A 203 (2003) 231.
[33] Z. Poltarzewski, S. Galvagno, R. Pietropaolo, P. Staiti, J. Catal. 102 (1986) 190.
[34] M.A. Aramendía, V. Boreau, C. Jiménez, J.M. Marinas, A. Porras, F.J. Urbano, J. Catal. 172 (1997) 46.
[35] W. Palczewska, Adv. Catal. 24 (1975) 245.
[36] R. Greenler, K. Burch, K. Kretzschmar, R. Klauser, A. Bradshaw, B. Hayden, Surf. Sci. 152–153 (1985) 338.
[37] S. Bertarione, D. Scarano, A. Zecchina, V. Johanek, J. Hoffmann, S. Schauermann, M.M. Frank, J. Libuda, G. Rupprechter, H.J. Freund, J. Phys. Chem. B 108 (2004) 3603.
[38] C. Binet, A. Jadi, J.C. Lavalley, J. Chim. Phys. 86 (3) (1989) 451.
[39] S. Verdier, B. Didillon, S. Morin, D. Uzio, J. Catal. 218 (2003) 288.
[40] A.F. Lee, C.J. Baddeley, M.S. Tikhov, R.M. Lambert, Surf. Sci. 373 (1997) 195.
[41] E. Merlen, P. Beccat, J.C. Bertolini, P. Delichère, N. Zanier, B. Didillon, J. Catal. 159 (1996) 178.
[42] S. Nishiyama, T. Hara, S. Tsuruya, M. Masai, J. Phys. Chem. B 103 (1999) 4431.
[43] A. Garron, K. Lázár, F. Epron, Appl. Catal. B 59 (2005) 57.
[44] G. Lafaye, C. Micheaud-Especel, C. Montassier, P. Marecot, Appl. Catal. A 230 (2002) 19.
[45] E.A. Sales, J. Jove, M.J. Mendes, F. Bozon-Verduraz, J. Catal. 195 (2000) 88.
[46] H. Berndt, I. Mönnich, B. Lücke, M. Menzel, Appl. Catal. B 30 (2001) 111.
[47] G.J. Blyholder, J. Phys. Chem. 68 (1964) 2772.
[48] J. Llorca, N. Homs, J. León, J. Sales, J.L.G. Fierro, P. Ramirez de la Piscina, Appl. Catal. A 189 (1999) 77.
[49] F.Z. Bentahar, J.P. Candy, J.M. Basset, F. Le Peltier, B. Didillon, Catal. Today 66 (2001) 303.
[50] S.M. Jung, E. Godard, S.Y. Jung, K.C. Park, J.U. Choi, Catal. Today 87 (2003) 171.